molecules

MDPI

Article

One-Step Fabrication of N,S-Codoped Carbon Dots from *Acronicta major* Larva: Structural Characterization and Sedative–Hypnotic Mechanisms

Kai Cheng [1,†], Xinrong Tian [1,†], Jinyu Ma [1,†], Ertong Dai [1], Ruiyan Liu [1], Minlong Xia [1], Bilin Jin [1], Siqi Wang [1], Zixuan Lu [1], Yue Zhang [2], Hui Kong [1,*], Huihua Qu [3,*] and Yan Zhao [1,*]

[1] School of Traditional Chinese Medicine, Beijing University of Chinese Medicine, Beijing 100029, China; chengkai199802@163.com (K.C.); tianxinrong9802@126.com (X.T.); majinyu0810@126.com (J.M.); 18561693155@163.com (E.D.); 13849303720@163.com (R.L.); 20240931022@bucm.edu.cn (M.X.); billion2024@163.com (B.J.); restat5pm@163.com (S.W.); luzixuan@163.com (Z.L.)
[2] School of Life Sciences, Beijing University of Chinese Medicine, Beijing 100029, China; 201801024@bucm.edu.cn
[3] Center of Scientific Experiment, Beijing University of Chinese Medicine, Beijing 100029, China
* Correspondence: doris7629@126.com (H.K.); quhuihuadr@163.com (H.Q.); zhaoyandr@163.com (Y.Z.); Tel.: +86-010-62486705 (H.K. & H.Q. & Y.Z.)
† These authors contributed equally to this work.

Abstract

The *Acronicta major* larva is a toxic agricultural pest that poses severe ecological management challenges. This study presents a sustainable strategy to valorize this hazardous biological waste into functional nanotherapeutics for insomnia by leveraging its unique intrinsic chemical composition. Carbon dots derived from *Acronicta major* larva (AM-CDs) were synthesized via one-step pyrolysis, which facilitated the natural molecular pre-assembly of N,S-codoping. Their physicochemical properties and cytotoxicity were evaluated using a series of characterizations and the CCK-8 assay. The sedative and hypnotic effects were assessed in mice with PCPA-induced insomnia through hot plate, Open Field and pentobarbital-induced sleep tests, and their potential mechanism was explored via neurotransmitter detection. The thermal process effectively eliminated intrinsic toxicity while retaining bioactivity via in situ heteroatom doping. AM-CDs exhibited favorable biocompatibility and significant sedative–hypnotic activity, reducing anxiety-related agitation without motor impairment. Mechanistically, AM-CDs effectively restored the GABA/5-HT/glutamate axis. Unlike direct central receptor binding, our findings suggest that this therapeutic effect is likely mediated through a systemic or peripheral regulatory pathway. This study demonstrates the conversion of toxic pests into safe and intrinsically bioactive nanomaterials, providing a dual solution for ecological pest management and novel neuroactive agent development, and validating the "Waste-to-Wealth" concept in biomedicine.

Keywords: carbon dots; *Acronicta major*; insomnia

Check for updates

Received: 5 January 2026
Revised: 9 February 2026
Accepted: 15 February 2026
Published: 23 February 2026

Copyright: © 2026 by the authors. Licensee MDPI, Basel, Switzerland. This article is an open access article distributed under the terms and conditions of the Creative Commons Attribution (CC BY) license.

1. Introduction

The management of hazardous forestry and agricultural pests represents a critical challenge in global ecological conservation [1]. Among these biological threats, the larvae of *Acronicta major* stand out as a unique category of hazardous biological waste [2]. As notorious polyphagous defoliators widely distributed in Asia, these pests inflict severe

damage on broad-leaved forests (e.g., poplar and willow), incurring substantial economic losses annually [3]. Unlike benign agricultural by-products (e.g., fruit peels), *Acronicta major* larvae possess negative economic value due to their biological toxicity; their body surface is covered with dense setae that can trigger dermatitis and allergic reactions in humans upon contact [4–6]. Traditionally, the interaction between humans and this pest is limited to costly chemical extermination and physical disposal, which often leads to secondary environmental pollution [7,8]. Therefore, transforming this toxic, abundant ecological burden into a functional material would not only mitigate a pest crisis but also represent a paradigm shift in high-value resource valorization.

In the pursuit of sustainable material synthesis, the conversion of biomass waste into carbon dots (CDs) has attracted significant attention [9]. CDs are ultra-small fluorescent nanoparticles known for their biocompatibility and tunable surface chemistry [10–12]. However, a critical limitation exists in current biomass-derived CDs: most conventional precursors (e.g., grass, wood, or cellulose) are chemically inert and composed primarily of carbon and oxygen. To achieve functional heteroatom doping (specifically nitrogen and sulfur) for enhanced bioactivity, researchers are often forced to add exogenous chemical dopants such as urea, ethylenediamine, or strong acids. This external doping strategy not only complicates synthesis but also introduces potential toxicity risks and results in heterogeneous doping sites. In contrast, the larva of *Acronicta major* constitutes a specialized biological reservoir of heteroatoms. Their bodies are composed of protein-rich tissues and chitin, which naturally contain high ratios of nitrogen (N) and sulfur (S). We hypothesize that this unique biological composition offers a natural molecular pre-assembly, where the heteroatoms are already chemically integrated into the precursor's structure. Through high-temperature pyrolysis, this hazardous organic matter can be transformed via an intrinsic self-doping mechanism. This process thermally degrades the thermolabile allergenic factors while doping the carbon lattice in situ with N and S atoms. This approach avoids the use of toxic external additives required by synthetic CDs, yielding a pure, N,S-codoped nanomaterial with superior surface polarity and biocompatibility. Such a transformation turns "waste" into "wealth," utilizing its intrinsic chemical composition to engineer functional nanomaterials without the need for external chemical dopants.

While the primary motivation is ecological valorization, the potential application of these insect-derived CDs finds inspiration at the intersection of nanotechnology and Traditional Chinese Medicine (TCM). TCM possesses extensive experience in the application of insect-derived medicines, with insects that are processed at high temperatures being frequently used to treat neurological disorders such as insomnia and epilepsy. Crucially, the traditional technique of carbonization is historically employed to detoxify poisonous plants and insects while changing or enhancing their therapeutic efficacy. Currently, insomnia and anxiety-related disorders are a pervasive global epidemic [13,14], yet standard treatments like benzodiazepines are hampered by dependence and tolerance [15,16]. Drawing on this concept, we postulate that the N,S-codoped carbonized derivatives of *Acronicta major*—owing to their enhanced redox capabilities and surface affinity—may possess inherent sedative–hypnotic properties.

Herein, we report a holistic strategy to radically transform the larva of *Acronicta major* from a forestry pest into a bioactive nanotherapeutic. Through a convenient one-step pyrolysis method, we synthesized AM-CDs derived from the larva of *Acronicta major*. This approach effectively strips the pest of its biological toxicity and identity, endowing it with completely new pharmacological properties, specifically, sedation and hypnosis, that the raw insect did not possess. This study serves primarily as a demonstration of "Waste-to-Wealth" conversion for hazardous biological waste, while simultaneously providing

modern scientific evidence for the neuro-modulatory potential of intrinsically doped insect-derived carbon nanomaterials.

2. Results

2.1. Synthesis and Characterization of AM-CDs

As shown in Figure 1A, the aqueous solution of AM-CDs exhibits a clear pale-yellow color under daylight. Figure 1B confirms the colloidal nature of the solution by observing a distinct red laser light path (Tyndall effect). Furthermore, under illumination with a 365 nm UV lamp, the AM-CD solution emits bright blue fluorescence, indicating its excellent photoluminescent properties.

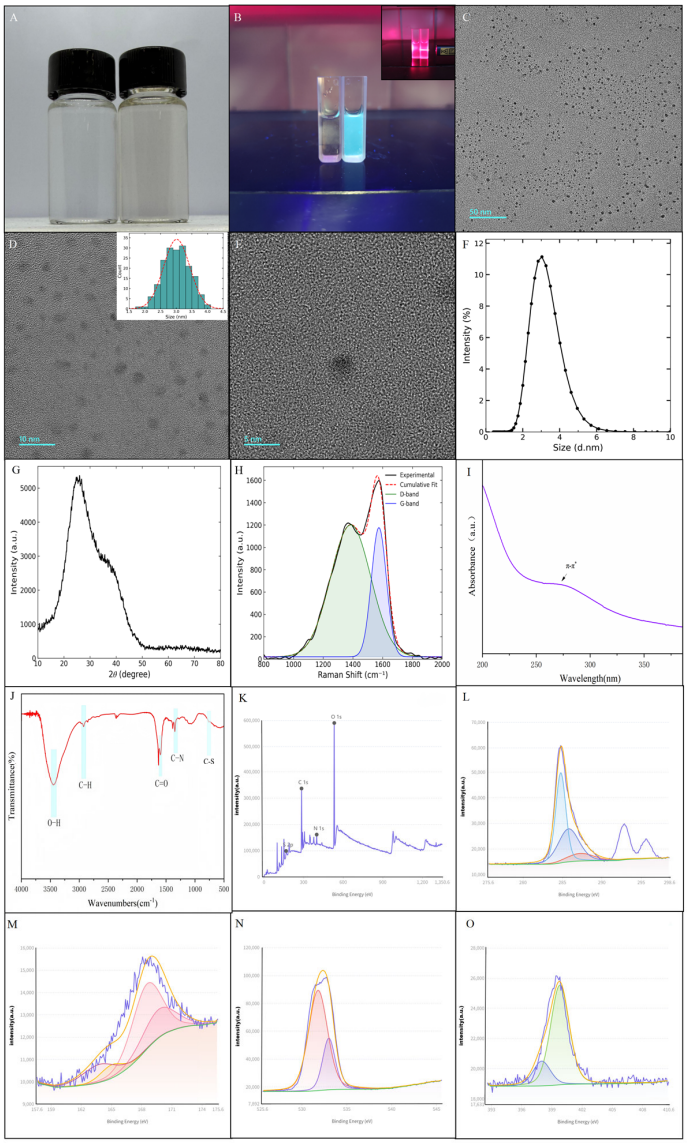


Figure 1. The characterization of AM-CDs. (**A**) Photographs of AM-CD aqueous solution under natural light. (**B**) The Tyndall effect observed under a red laser beam and bright blue fluorescence emitted under 365 nm UV irradiation. (**C**,**D**) TEM images at different magnifications and a statistical histogram based on particle counting. (**E**) HRTEM image of AM-CDs. (**F**) Particle size distribution of AM-CDs. (**G**) XRD patterns of AM-CDs. (**H**) Raman spectra of AM-CDs. (**I**) UV−Vis absorption spectrum of AM-CDs. (**J**) FTIR spectrum of AM-CDs. (**K**) XPS full survey scan spectrum of AM-CDs. (**L**–**O**) High-resolution XPS spectra corresponding to (**L**) C 1s, (**M**) S 2p, (**N**) O 1s, and (**O**) N 1s.

In Figure 1C,D, TEM observations reveal that the synthesized AM-CDs exhibit a uniform spherical morphology in aqueous solution and demonstrate excellent monodispersity

in aqueous solutions without significant aggregation. The statistical histogram based on particle counting indicates that the lateral diameters of AM-CDs are mainly distributed in the range of 2.0–4.0 nm, with an average diameter of approximately 3.0 nm. Figure 1E displays a HRTEM image revealing discernible lattice fringes within the AM-CDs. The clearly defined lattice striations indicate that AM-CDs contain crystalline graphite-like domains. To further evaluate the dispersion behavior in the aqueous state, dynamic light scattering (DLS) measurements were conducted (Figure 1F). The results display a narrow size distribution with an average hydrodynamic diameter of 3.04 nm. This value is comparable to the TEM statistical results, suggesting that the AM-CDs possess a compact hydration shell and exist as monodisperse individual particles in aqueous solution with high colloidal stability.

To further corroborate the crystalline phase and investigate the structural defects of the AM-CDs, XRD and Raman spectroscopy analyses were performed. As shown in Figure 1G, the XRD pattern displays a broad diffraction peak centered at $2\theta = 26.0^{\circ}$, corresponding to the typical lattice plane of graphitic carbon. The calculated interlayer spacing is approximately 0.34 nm, which is slightly larger compared to that of bulk graphite (0.335 nm). This lattice expansion may be attributed to the turbostratic nature of the carbon, where the intercalation of abundant heteroatoms (N and S) and surface functional groups enlarges the distance between the graphitic layers.

Complementary to XRD, the Raman spectrum (Figure 1H) provides insights into the electronic structure and defect density. Two characteristic peaks are clearly observed: the D-band at 1380 cm^{-1} (associated with sp3 hybridized disordered carbon or structural defects) and the G-band at 1580 cm^{-1} (associated with the in-plane vibration of sp2 graphitic carbon). The calculated intensity ratio (ID/IG) is 1.02. This moderate ratio suggests a hybrid structural feature: the AM-CDs possess graphitic domains (evidenced by the distinct G-band and HRTEM lattice fringes) that ensure stable fluorescence emission, while simultaneously retaining abundant surface defects and edge states (as indicated by the prominent D-band). These "defects" effectively correspond to the N/S-doping sites and surface edges, which are critical for water dispersibility and biological interactions.

The UV-Vis profile (Figure 1I) shows a distinct peak around 270 nm, which is ascribed to the π-π^* transition of the aromatic sp2 carbon domains. To comprehensively elucidate the surface chemical landscape and the structural origins of the physicochemical properties of AM-CDs, FTIR and XPS analyses were conducted. The FTIR spectrum (Figure 1J) reveals that the AM-CDs inherit abundant functional groups from the biological precursors (*Acronicta major* larvae). The broad absorption band at ~3400 cm^{-1} corresponds to the stretching vibrations of O–H and N–H, while the sharp peaks at 1630 cm^{-1} and 1400 cm^{-1} are attributed to C=O (Amide I) and C–N stretching vibrations, respectively. Additionally, the characteristic vibration bands at 2900 cm^{-1} (C–H) and ~750 cm^{-1} (C–S) further confirm the preservation of the carbon backbone and the successful incorporation of sulfur. Critically, the presence of these abundant hydrophilic functionalities (hydroxyl, carboxyl, and amino groups) on the surface imparts excellent water dispersibility and biocompatibility to the AM-CDs, which is a prerequisite for their subsequent application in biological systems.

Complementary to FTIR, XPS measurements were employed to provide quantitative insights into the chemical bonding states and doping mechanism. The wide-scan spectrum (Figure 1K) clearly identifies C (52.92%), N (4.69%), O (38.54%), and S (3.85%), confirming the codoped composition. The high-resolution C 1s spectrum (Figure 1L) can be deconvoluted into three components at 284.8, 285.8, and 287.3 eV, corresponding to sp^2 graphitic carbon (C–C/C=C), C–N/C–S, and C=O bonds, respectively. This indicates that AM-CDs possess a carbonaceous core structure decorated with heteroatom-containing functional groups. The O 1s spectrum (Figure 1N), resolved into peaks at 531.8 eV (C=O)

and 533.0 eV (C–O–C/C–OH), further corroborates the oxygen-rich surface state derived from the oxidation of biomass during pyrolysis.

Most importantly, the detailed analysis of N and S states reveals the intrinsic mechanism of the optical properties. The N 1s spectrum (Figure 1O) shows two dominant configurations: pyridinic N (398.0 eV) and pyrrolic N (399.8 eV). The high proportion of pyridinic nitrogen is significant, as it contributes p-electrons to the π-conjugated system, thereby introducing new energy levels and enhancing the fluorescence quantum yield. Furthermore, the S 2p spectrum (Figure 1M) displays doublet peaks characteristic of thiophene-type sulfur (-C-S-C-) and oxidized sulfur (168–169 eV). The formation of thiophene-S confirms that sulfur atoms are covalently doped into the aromatic framework, stabilizing the carbon structure, while the oxidized sulfur species further enhances the surface hydrophilicity. In summary, the specific N,S-codoped conjugated structure and the rich surface functionalization synergistically contribute to the robust fluorescence stability and low cytotoxicity of the AM-CDs.

2.2. Evaluation of Central-like Analgesic and Sedative Efficacy

To evaluate the potential sedative and antinociceptive effects of AM-CDs, the hot plate test was performed at 1 h and 2 h post-administration. As shown in Tables 1 and 2, the saline control group exhibited stable baseline pain latency, with values of 14.35 ± 1.44 s at 1 h and 12.48 ± 1.53 s at 2 h. In contrast, the positive control group (morphine, 10 mg/kg) displayed a robust and sustained central analgesic effect, significantly increasing the latency of pain to 31.34 ± 11.73 s at 1 h and 30.97 ± 6.06 s at 2 h ($p < 0.001$).

Notably, AM-CDs induced a rapid, dose-dependent elevation in a nociceptive threshold. At 1 h post-administration, the high-dose AM-CDs group prolonged pain latency to 29.1 ± 5.15 s ($p < 0.01$), achieving a peak efficacy statistically comparable to that of morphine. The medium-dose group (17.11 ± 6.23 s) showed a non-significant increase, while the low-dose group (11.51 ± 3.24 s) exhibited a slight decrease compared to the control.

At 2 h, the high-dose AM-CDs group maintained a significantly higher pain threshold (22.37 ± 9.86 s, $p < 0.05$) relative to the control, though the effect was slightly attenuated and lower than that of the morphine group. The medium-dose group (12.79 ± 6.48 s) remained near the baseline, while the low-dose group (15.27 ± 4.54 s) showed a mild, non-significant increase in latency. This temporal profile—characterized by a rapid onset and potent peak effect—strongly suggests that AM-CDs possess significant systemic antinociceptive activity. While functionally mimicking the profile of central analgesics, this effect provides the phenotypic basis for their sedative properties, which we hypothesize involves the modulation of neuro-active pathways via systemic regulation.

Table 1. Hot plate test at 1 h post-administration.

Group	Number of Animals (*n*)	Pain Threshold (s)
Control	8	14.35 ± 1.44
Morphine	8	31.34 ± 11.73 ***
High Dose	8	29.1 ± 5.15 **
Medium Dose	8	17.11 ± 6.23
Low Dose	8	11.51 ± 3.24

Notes: Data are presented as mean ± SD ($n = 8$). ** $p < 0.01$, *** $p < 0.001$ vs. control group.

Table 2. Hot plate test at 2 h post-administration.

Group	Number of Animals (*n*)	Pain Threshold (s)
Control	8	12.48 ± 1.53
Morphine	8	30.97 ± 6.06 ***
High Dose	8	22.37 ± 9.86 *
Medium Dose	8	12.79 ± 6.48
Low Dose	8	15.27 ± 4.54

Notes: Data are presented as mean ± SD (n = 8). * $p < 0.05$, *** $p < 0.001$ vs. control group.

2.3. Behavioral Regulation in PCPA-Induced Insomnia Model

The sedative and anxiolytic effects of AM-CDs were comprehensively evaluated in the PCPA-induced insomnia model using the Open Field Test (OFT). Five key kinematic and spatial parameters were analyzed: Total Distance Traveled, Average Velocity, Frequency of Center Entries, and Cumulative Duration in the Center and Periphery.

Visual analysis of representative trajectory plots and heatmaps (Figure 2A,B) revealed distinct behavioral patterns among the groups. The normal control mice exhibited a balanced exploration of the entire arena, characterized by a prominent high-intensity "hot spot" in the center of the heatmap. In stark contrast, the PCPA-treated model mice displayed chaotic movement trajectories strictly confined to the peripheral zone (thigmotaxis), leaving a cold void (dark blue area) in the center with high-intensity hot spots concentrated solely in the corners, indicating severe psychomotor agitation and anxiety.

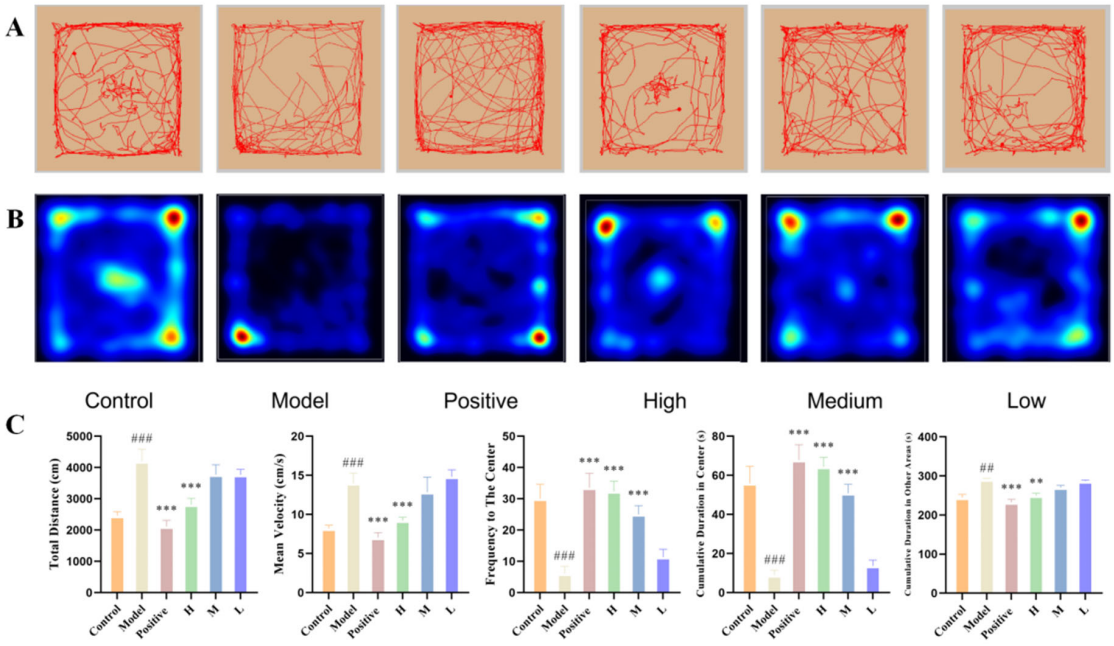


Figure 2. Effects of AM-CDs on spontaneous locomotor activity and anxiety-like behaviors in PCPA-treated mice (Open Field Test). (**A**) Representative motion trajectories of mice from different experimental groups over a 5 min session. (**B**) Corresponding heatmaps visualizing the spatial distribution and dwell-time density. Warmer colors (red/yellow) indicate higher time spent in that area, while cooler colors (blue) indicate less time spent in an area. (**C**) Quantitative analysis of behavioral parameters, including Total Distance, Mean Velocity, Frequency of Entries into the Center, and Cumulative Duration in the Center. Data are presented as mean ± SD (n = 8). ### $p < 0.001$, ## $p < 0.01$ vs. control group; *** $p < 0.001$, ** $p < 0.01$ vs. model group.

Crucially, treatment with AM-CDs (at a high dose) remarkably reversed this anxiety-like phenotype. As evidenced by the heatmaps, the high-dose group exhibited the re-emergence of a distinct, high-intensity hot spot in the central zone, a pattern that closely

mirrors the normal control group and demonstrates a superior restoration of exploratory behavior compared to the medium- and low-dose groups. This visual evidence confirms that high-dose AM-CDs effectively overcame the thigmotactic behavior induced by PCPA.

Quantitative analysis (Figure 2C) confirmed these observations. Regarding locomotor activity, the model group showed a state of over-excitement, characterized by a significant increase in Total Distance (4192.89 ± 397.56 cm, $p < 0.01$) and Average Velocity (13.97 ± 1.33 cm/s, $p < 0.01$) compared to the normal control. Treatment with AM-CDs effectively mitigated this hyperactivity. The high-dose group significantly reduced the Total Distance to 2460.52 ± 181.42 cm ($p < 0.01$) and Average Velocity to 8.20 ± 0.60 cm/s ($p < 0.01$), restoring them to near-physiological levels. Regarding anxiety-related behaviors, the model group exhibited a marked reduction in both the Frequency of Center Entries (6 times) and Center Time (8.90 ± 2.61 s), accompanied by a prolonged Peripheral Time (291.1 ± 2.61 s), reflecting heightened anxiety levels. Crucially, treatment with AM-CDs reversed this anxiety-driven phenotype. The high-dose group significantly increased the number of Center Entries to 24 times and extended the Center Time to 50.61 ± 6.45 s ($p < 0.01$), while correspondingly decreasing the Peripheral Time to 249.39 ± 6.45 s. Collectively, these results indicate that AM-CDs effectively alleviate insomnia-associated agitation and anxiety, promoting a calm yet alert behavioral state without inducing catalepsy.

2.4. Synergistic Hypnotic Effects with Pentobarbital

The hypnotic efficacy of AM-CDs was quantified by measuring sleep latency and duration in PCPA-insomniac mice following a sub-threshold/threshold dose of pentobarbital sodium. As shown in Table 3, the model group displayed severe sleep disturbances, characterized by a prolonged sleep latency of 7.88 ± 1.06 min ($p < 0.01$) and a shortened sleep duration of 5.88 ± 0.92 min ($p < 0.001$) compared to the normal control.

Table 3. Effects of PCPA and drug interventions on pentobarbital-induced sleep in mice.

Group	Sleep Latency (min)	Sleep Duration (min)
Control	6.32 ± 1.81	65.76 ± 2.13
Model	7.88 ± 1.06 $^{\#\#}$	5.88 ± 0.92 $^{\#\#\#}$
Positive	5.39 ± 0.36 ***	104.38 ± 9.22 ***
High Dose	6.04 ± 0.65 **	31.49 ± 4.24 **
Medium Dose	7.03 ± 0.87	17.27 ± 1.63
Low Dose	7.78 ± 0.47	6.93 ± 0.79

Notes: Data are presented as mean ± SD ($n = 8$). ** $p < 0.01$, *** $p < 0.001$ vs. model group. $^{\#\#}$ $p < 0.01$, $^{\#\#\#}$ $p < 0.001$ vs. control group.

Administration of AM-CDs exerted a potent synergistic effect with pentobarbital. The high-dose group significantly shortened sleep latency to 6.04 ± 0.65 min ($p < 0.01$) and prolonged sleep duration to 31.49 ± 4.24 min ($p < 0.01$). This dose-dependent improvement reversed the PCPA-induced insomnia phenotype. It is noteworthy that high doses of AM-CDs exhibit hypnotic effects similar to those of diazepam. However, diazepam demonstrates a significant advantage in prolonging sleep duration, suggesting that AM-CDs may promote sleep onset and enhance sleep maintenance through central nervous system regulation.

2.5. Modulation of Neurotransmitter Levels

To elucidate the molecular mechanism underlying the observed sedative–hypnotic effects, the levels of key neurotransmitters were analyzed via ELISA. As illustrated in Figure 3, PCPA treatment effectively disrupted the neurochemical balance, resulting in

significantly reduced levels of inhibitory neurotransmitters (5-HT and GABA) and elevated levels of the excitatory neurotransmitter (glutamate) compared to the normal control.

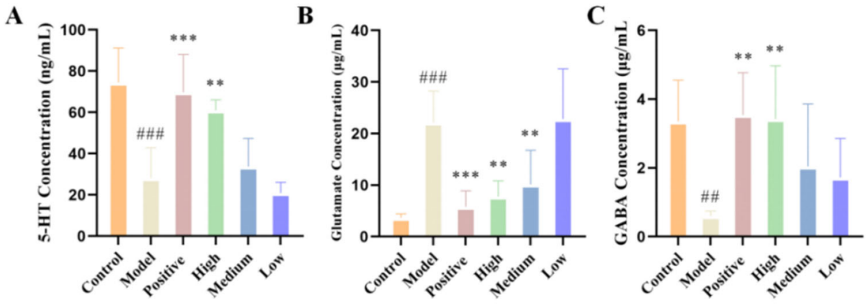


Figure 3. Modulation of neurotransmitter levels by AM-CDs in PCPA-induced insomniac mice. (**A**) 5-HT, (**B**) Glu, and (**C**) GABA. Data are presented as mean ± SD (n = 8). $^{\#\#}$ $p < 0.01$, $^{\#\#\#}$ $p < 0.001$ vs. control group; *** $p < 0.001$, ** $p < 0.01$ vs. model group.

Treatment with AM-CDs effectively restored this excitatory–inhibitory equilibrium. Specifically, the levels of 5-HT and GABA in the high-dose group were upregulated to 60.95 ± 5.16 ng/mL and 3.42 ± 1.54 ng/mL, respectively, which is significantly higher than those in the model group ($p < 0.01$). Concurrently, the concentration of glutamate was downregulated from 22.15 ± 6.10 ng/mL (model group) to 7.79 ± 3.04 ng/mL (high-dose group), attenuating excessive excitatory neurotransmission associated with insomnia. These findings confirm that AM-CDs function by modulating the GABA/Glu/5-HT axis, enhancing an inhibitory tone while dampening excitatory drive.

2.6. In Vitro Biocompatibility Evaluation

Prior to in vivo application, the cytotoxicity of AM-CDs was assessed in RAW 264.7 cells using the CCK-8 assay. As shown in Figure 4, after 6 h of incubation, cells maintained high survival rates (>90%) across a broad concentration range from 7.81 to 1000 μg/mL. Even at the highest tested concentration (1000 μg/mL), no significant cell death was observed compared to the control group. After 12 h, 24 h and 72 h incubation periods, cell viability fell below 90% at 1000 μg/mL, while all other concentration ranges maintained high viability above 90%. This exceptional biocompatibility indicates that AM-CDs exhibit low biotoxicity, validating their safety for potential biomedical applications. Consequently, AM-CDs demonstrate broad application prospects in the pharmaceutical field.

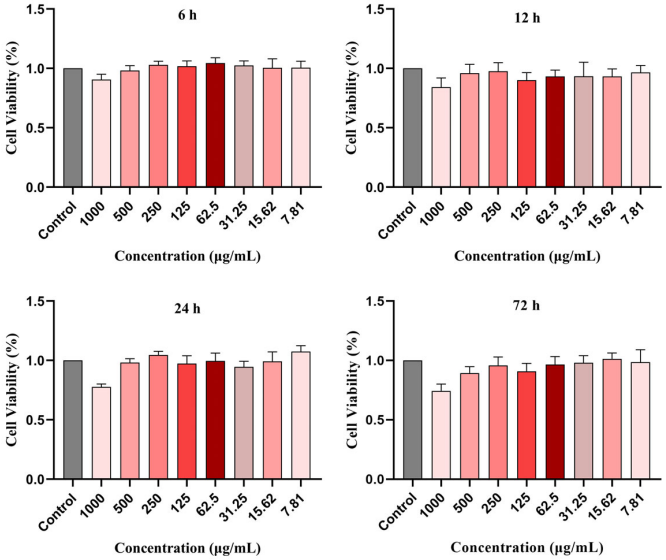


Figure 4. Effect of different concentrations of AM-CDs on cell viability for the RAW264.7 macrophage for 6 h, 12 h, 24 h, and 72 h.

3. Discussion

The dual challenges of sustainable pest management and the search for safer sedative therapeutics have seemingly disparate solutions. However, this study bridges these domains by demonstrating a novel "Waste-to-Wealth" strategy that fundamentally alters the value proposition of a notorious agricultural and forestry pest. In its native form, the *Acronicta major* larva is a negative-value form of biological waste characterized by allergenic dense setae and inflammatory toxins. Our results confirm that the programmed pyrolysis strategy acts as a robust purification mechanism, converting a toxic precursor into a biocompatible material. Thermal treatment (reaching 350 °C) denatured the protein-based toxins and degraded the allergenic structures, converting the pest into AM-CDs. Crucially, the biocompatibility assays confirmed that this transformation effectively eliminates biological toxicity, as evidenced by the high viability of RAW 264.7 cells even at high concentrations. This validates a radical shift in ecological management: instead of costly physical disposal or chemical extermination, these pests can be reclaimed as pre-assembled biological precursors for high-value functional nanomaterials.

The distinct advantage of utilizing *Acronicta major* larva over abundant plant biomass stems from the molecular-level compositional superiority of the insect precursor. While plant-derived waste is typically cellulosic and often requires toxic external nitrogen sources (e.g., urea or ethylenediamine) to achieve functional doping [17–19], the insect body is intrinsically enriched with proteins and chitin [19,20]. Spectroscopic analyses via XPS and FTIR confirmed that these biological heteroatoms were successfully incorporated into the carbon lattice during pyrolysis, yielding high concentrations of nitrogen (4.69%) and sulfur (3.85%). This represents a "natural molecular pre-assembly," where the heteroatoms are in situ-doped into the carbon framework, avoiding the structural heterogeneity often caused by physical mixing of external dopants. Notably, the generation of specific nitrogen states is critical; these surface defects function as electron donors or acceptors [21], potentially creating active sites that underpin the material's redox and metabolic regulatory capabilities. Consequently, the *Acronicta major* larva serves not merely as a carbon source, but as an integrated reservoir for intrinsic heteroatom doping that confers unique bioactivity to the resulting AM-CDs.

To elucidate the pharmacological nature of AM-CDs, it is imperative to distinguish between peripheral physiological effects and central neurological modulation. The hot plate test, employing morphine as a positive control, served as the primary diagnostic tool for establishing this central activity [22–24]. Unlike chemical writhing tests that often reflect peripheral anti-inflammatory mechanisms [25], the thermal nociception in the hot plate assay is governed by complex processing at spinal and supraspinal levels [26]. The observation that AM-CDs significantly prolonged pain latency, mirroring the central analgesic profile of morphine, provides compelling evidence that AM-CDs are capable of modulating nociceptive signaling pathways usually associated with the central nervous system. In neuropharmacology, such an elevation in the nociceptive threshold, particularly in the absence of anti-inflammatory agents, is frequently a concomitant manifestation of sedation and neural system regulation [27,28].

This sedative capacity was further validated in a PCPA-induced insomnia model, which represents the pathological state of excessive central neuronal excitation driven by 5-HT depletion [29,30]. In the Open Field Test, the PCPA-treated mice exhibited characteristic psychomotor agitation and anxiety-driven hyper-locomotion, reflecting a severe disruption of the excitatory–inhibitory balance [31]. Crucially, the administration of AM-CDs effectively attenuated this pathological excitability. Rather than causing indiscriminate suppression of locomotor activity, the treatment specifically modulated the behavioral phenotype, restoring exploratory patterns and dwell time in the central zone to near-normal

physiological levels. This demonstrates that AM-CDs function as a potent regulator of sleep–wake homeostasis, alleviating the symptoms of insomnia and anxiety by modulating an overall neural tone, without inducing the profound catalepsy often associated with non-selective synthetic sedatives.

To elucidate the molecular pathways underlying these behavioral phenotypes, we conducted neurotransmitter-related analyses. Since PCPA induces a state of excessive central neuronal excitation, specifically via the enzymatic depletion of 5-HT [32], the observed therapeutic efficacy of AM-CDs points to the regulation of the GABA/Glu/5-HT neurochemical axis. Specifically, AM-CDs significantly reversed the PCPA-induced pathological deficits in 5-HT and GABA. Given that GABA serves as the primary inhibitory neurotransmitter governing sleep initiation, its restoration is pivotal [33,34]. However, regarding the precise mode of action, we adopted a cautious interpretation. Previously, it might be hypothesized that the abundant surface functional groups (e.g., carboxyl and amino moieties) of AM-CDs could directly interact with receptors. Yet, considering the high hydrophilicity and negative surface charge of AM-CDs, which hinder passive BBB diffusion, we propose that the observed neurotransmitter restoration is likely mediated through systemic or peripheral modulation rather than direct central receptor binding. The N/S-doped surface chemistry of AM-CDs may act as a "peripheral sink" to mitigate systemic stress or modulate gut–brain signaling, subsequently influencing the central GABAergic and serotonergic tone indirectly. Concurrently, the treatment effectively downregulated glutamate levels, thereby dampening the excessive cortical excitotoxicity associated with insomnia. By systemically rebalancing the excitatory–inhibitory equilibrium, AM-CDs facilitate a natural transition into sleep, functionally distinguishing their mechanism from the global neuronal suppression often induced by conventional non-selective hypnotics [35,36].

Synthesizing the physicochemical characterization (TEM, XRD, Raman, and XPS) with the pharmacodynamic findings, the potent sedative–hypnotic efficacy of AM-CDs can be attributed to the cooperative interplay of their integrated structural features (as evidenced by the conjugated carbon framework in XRD and rich surface chemistry in XPS), which establishes a critical structure–activity relationship. This physicochemical foundation is strictly governed by the systemic regulatory pathway discussed above.

First, the FTIR and XPS results confirm that the AM-CDs possess a highly hydrophilic surface decorated with abundant functional groups (hydroxyl, carboxyl, and amides) derived from protein-rich *Acronicta major* precursors. These polar moieties act as "biological stabilizers," imparting excellent water dispersibility. Simultaneously, the carbonaceous framework identified by XRD ensures the structural integrity of these nanoparticles in the physiological environment. Unlike traditional hydrophobic drugs that require carriers, the amphiphilic nature and ultra-small size (~3 nm) of AM-CDs ensure high bioavailability and prolonged circulation time in the peripheral blood system. This stability is a prerequisite for AM-CDs to function as systemic regulators, allowing them to effectively modulate the peripheral pools of neurotransmitters (e.g., 5-HT or GABA precursors), which can indirectly influence central neuronal excitability.

Second, the intrinsic bioactivity of AM-CDs is fundamentally driven by the successful doping of nitrogen (4.69%) and sulfur (3.85%) into the carbon lattice. As revealed by XPS, the high proportion of pyridinic nitrogen and thiophene-sulfur significantly modifies the electronic landscape of the conjugated system. This observation aligns perfectly with the Raman spectroscopic results (ID/IG = 1.02), where detected lattice defects act as electron-rich active sites [37]. Instead of binding directly to CNS receptors, nitrogen doping creates localized electron-rich domains capable of interacting with circulating metabolic substrates or enzymes via hydrogen bonding or electrostatic attraction [38,39]. The codoping of sulfur introduces lattice distortion and spin-density changes, which endow the material with

potential robust redox capabilities, essential for scavenging systemic oxidative stress factors that often underlie insomnia pathology.

Therefore, the significant modulation of the GABA/Glu/5-HT axis observed in our study is not accidental but a direct consequence of this specific surface and electronic chemistry. Rather than necessitating the direct crossing of the blood–brain barrier (BBB) to bind central receptors, we propose that AM-CDs likely act by regulating the peripheral equilibrium of these neurotransmitters. By protecting inhibitory transmitters (GABA, 5-HT) from rapid metabolic degradation or modulating their peripheral synthesis/transport in the circulatory system, AM-CDs exert a "bottom-up" regulatory effect that ultimately propagates to the central nervous system. This validates the fact that AM-CDs act as bioactive nanomedicines with intrinsic therapeutic potential, driven by the specific N/S-codoped structure inherited from the molecular pre-assembly of the *Acronicta major* larva.

Despite the excellent optical properties and sedative–hypnotic efficacy of the AM-CDs, limitations of the preparation method should be acknowledged. First, the mass yield of AM-CDs via the top-down pyrolysis of *Acronicta major* larvae is relatively limited due to the significant formation of non-fluorescent carbon residues during carbonization. Second, although the programmed multi-step heating ensures structural uniformity, the subsequent purification process—specifically 72 h of dialysis—is time-consuming, which may constrain rapid large-scale production. Future research efforts will focus on optimizing the carbonization parameters and exploring more efficient purification techniques to improve the yield and production efficiency of biomass-derived carbon dots.

Finally, this study bridges the empirical wisdom of TCM with the modern imperative of sustainable resource utilization. Historically, processed insects have been employed to regulate the central nervous system, representing an early type of biological resource valuation. Our findings suggest that the therapeutic efficacy of such traditional preparations likely stems from the unintentional formation of bioactive carbon nanoclusters. By refining this crude technique into a controlled pyrolytic synthesis, we successfully upcycled a hazardous agricultural pest into standardized AM-CDs. This approach not only elucidates the material basis of carbonized biomass but also revitalizes ancient pharmacopeia through the lens of green nanotechnology, offering a dual solution for ecological management and drug discovery.

4. Materials and Methods

4.1. Materials

Acronicta major larvae were collected from the campus of Beijing University of Chinese Medicine and identified by the researcher Qu Huihua. p-Chlorophenylalanine (PCPA, CAS No. 7424-00-2) was purchased from Acima Biotechnology Co., Ltd. (Beijing, China). Pentobarbital sodium (CAS No. 57-33-0) was obtained from Sigma Co., LLC. (St. Louis, MO, USA). Morphine (Batch No. 161109-1) was supplied by Nanjing Bai Jingyu Pharmaceutical Co., Ltd. (Nanjing, China). ELISA kits for γ-aminobutyric acid (GABA; Cat. No. ml570049M), 5-hydroxytryptamine (5-HT; Cat. No. ml-E-22296), and glutamate (Glu; Cat. No. ml203551M) were acquired from Shanghai Enzyme-Linked Biotechnology Co., Ltd. (Shanghai, China). Dialysis membranes (Cat. No. HF132640-1m; molecular weight cutoff: 1000 Da) were purchased from Beijing Ruida Henghui Technology Development Co., Ltd. (Beijing, China). All experimental procedures were performed using deionized water.

4.2. Preparation of AM-CDs

Drawing on previous experience, we prepared AM-CDs through a programmed multi-step pyrolysis process. As illustrated in Figure 5, first, the collected *Acronicta major* larvae are dried. Second, the dried *Acronicta major* larvae is placed into a crucible and prepared

through programmed thermal treatment in a muffle furnace: initial heating was conducted at 200 °C over 10 min with a 30 min isothermal hold, followed by a secondary ramp to 300 °C over 10 min with a 30 min stabilization period, and a final ramp to 350 °C over 10 min with a 60 min isothermal hold. The carbonized product was cooled to ambient temperature and mechanically pulverized into fine powder. The powder was then homogenized with deionized water at a 1:30 (*w*/*v*) ratio and subjected to a 1 h heating extraction at 100 °C under controlled boiling conditions. The resulting solution was then vacuum-filtered through a 0.22 μm aqueous micropore membrane. For further purification, the solution was dialyzed against deionized water using a 1000 Da molecular weight cutoff (MWCO) membrane for 72 h, with regular replacement of the external medium until the solution became optically clear, which was stored at 4 °C for further use.

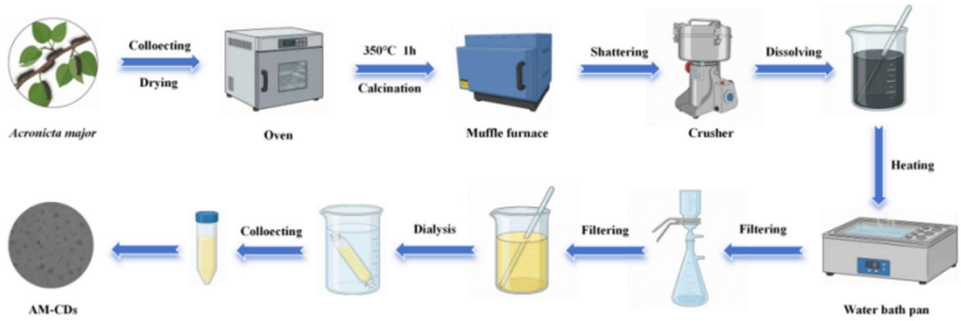


Figure 5. Brief diagram for AM-CD extraction and preparation.

4.3. Characterization of AM-CDs

The morphology and size of the AM-CDs were characterized using a JEM-2100F transmission electron microscope (Tokyo, Japan) (TEM, 200 kV). For TEM preparation, the AM-CD aqueous solution was diluted, filtered through a 0.22 μm membrane, sonicated for 5 min, and air-dried on a copper grid. The hydrodynamic diameter and polydispersity in the aqueous state were analyzed using a Zetasizer Lab (Malvern Panalytical, Malvern, UK) dynamic light scattering (DLS) system. To determine the crystalline structure and defect density, X-ray diffraction (XRD) patterns were recorded on a Bruker D8 Advance diffractometer (Karlsruhe, Germany) from 10° to 80°, and Raman spectra were acquired on a Horiba LabRAM HR Evolution spectrometer (Kyoto, Japan). The surface chemical composition and valence states were investigated by X-ray photoelectron spectroscopy (XPS) using a Thermo Scientific K-Alpha spectrometer (Waltham, MA, USA). Fourier transform infrared (FTIR) spectroscopy was performed on a Nicolet 6700 spectrometer (Waltham, MA, USA) (KBr pellet method). The optical properties of the diluted AM-CDs solution were measured using a TU-1991 UV-vis spectrophotometer and a Shimadzu RF-5301 PC spectrofluorimeter (Kyoto, Japan).

4.4. Animals

Male KM mice (20.0 ± 2.0 g) were purchased from Beijing Sibeifu Biotechnology (Beijing, China). Experiments were approved by the Committee of Ethics of Animal Experimentation of Beijing University of Chinese Medicine. Mice were housed under standard conditions (24 ± 1 °C, 55–65% humidity, 12 h light/dark cycle) with ad libitum access to food and water.

4.5. Hot Plate Test

To evaluate the central sedative/analgesic threshold, normal mice were randomly divided into five groups: the control group (Saline, i.p.), the positive group (morphine, 10 mg/kg, s.c.), and AM-CD groups (low, 0.12 mg/kg, medium, 0.24 mg/kg, and high doses, 0.48 mg/kg, i.p.). Mice underwent the hot plate test at 1 h and 2 h post-administration,

with a 24 h interval between trials. The hot plate was maintained at 55 ± 0.5 °C, and the latency to the first pain response (hind paw licking or jumping) was recorded.

4.6. Experimental Design and PCPA-Induced Insomnia Model

One week after the hot plate test was completed, mice were randomly divided into six groups: normal control group: treated with alkaline saline (i.p.) + distilled water (i.g.); model group: treated with PCPA (450 mg/kg, i.p.) + distilled water (i.g.); positive control group: treated with PCPA (450 mg/kg, i.p.) + diazepam suspension (1.5 mg/kg, i.g.); AM-CD low-dose group: treated with PCPA (450 mg/kg, i.p.) + AM-CDs (0.24 mg/kg, i.g.); AM-CD medium-dose group: treated with PCPA (450 mg/kg, i.p.) + AM-CDs (0.48 mg/kg, i.g.); and AM-CD high-dose group: treated with PCPA (450 mg/kg, i.p.) + AM-CDs (0.96 mg/kg, i.g.).

The PCPA-induced insomnia model was established by depleting serotonin. Except for the normal control group, mice were intraperitoneally (i.p.) injected with a PCPA suspension (450 mg/kg, prepared in alkaline physiological saline) once daily for 2 consecutive days. The normal control group received an isometric injection of alkaline physiological saline. Thirty-six hours after the completion of modeling, the behavioral manifestations of the mice were observed. The model was considered successfully established when mice exhibited symptoms such as hyperactivity, irritability, loss of circadian rhythm, and continuous activity during both the day and night.

Following successful modeling, mice in the drug treatment groups were administered the corresponding drugs via intragastric gavage (i.g.) once daily for 7 consecutive days. The normal control and model groups were administered an equivalent volume of distilled water.

4.7. Open Field Test (OFT)

The Open Field Test (OFT) was utilized to evaluate the autonomous locomotor activity and anxiety-like behaviors of the mice. The testing apparatus comprised a square enclosure measuring 50 × 50 cm^2. For each trial, the subject was positioned in the middle of the field, and its trajectory was monitored for a duration of 5 min using an automated video-tracking interface. To evaluate the sedative and anxiolytic effects of AM-CDs, specific behavioral metrics were quantified, including Total Distance Traveled, Cumulative Time Spent in the Central Zone, and Locomotor Speed of the Mice.

4.8. Pentobarbital-Induced Sleep Test

A total of 24 h after the Open Field Test, a pentobarbital-induced sleep experiment was conducted. Each mouse received an intraperitoneal injection of 2% pentobarbital sodium at a dose of 40 mg/kg. The experiment quantified two parameters: sleep latency (the duration from drug administration to the loss of the righting reflex) and sleep duration (the interval between sleep latency and the recovery of the righting reflex). Sleep onset was confirmed when the mouse remained in a supine position. To rigorously define awakening, a "double-confirmation" protocol was applied: upon the first successful righting, the mouse was immediately placed on its back again. The recovery time was recorded only if the mouse righted itself a second time within 60 s. Failure to do so resulted in the continuation of the sleep duration timing until this criterion was met. The entire process of animal experimentation is illustrated in Figure 6.

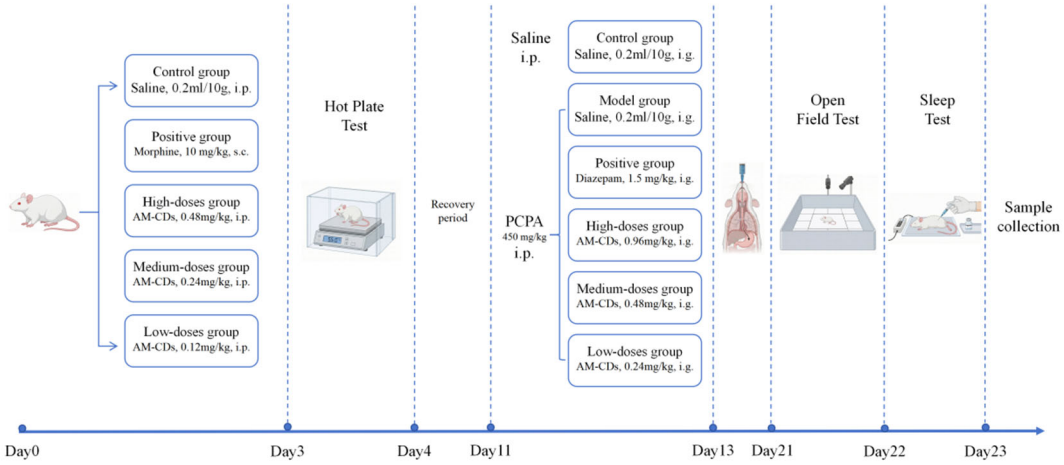


Figure 6. Diagram of the animal experimental procedure.

4.9. Sample Collection

Following a 24 h recovery period post-experiment, mice were anesthetized with sodium pentobarbital (40 mg/kg, i.p.). Blood samples were immediately obtained via the retroorbital sinus. Subsequently, the animals were sacrificed by decapitation while under deep anesthesia. The brain tissues were promptly dissected on ice, washed with cold saline to eliminate residual blood, weighed, and flash-frozen in liquid nitrogen. All samples were stored at −80 °C until biochemical analysis.

4.10. Determination of Neurotransmitters

After mechanically dissociating the frozen tissue in a pre-chilled environment, the brain homogenate was centrifuged to obtain the supernatant. The levels of neurotransmitters, including 5-hydroxytryptamine (5-HT), aminobutyric acid (GABA), and glutamate (Glu), were quantified using commercial ELISA kits strictly following the manufacturer's protocols.

4.11. In Vitro Cytotoxicity Assay

RAW 264.7 macrophages were maintained in DMEM supplemented with 10% FBS and antibiotics (100 IU/mL penicillin and 100 mg/mL streptomycin) under standard conditions (37 °C, 5% CO_2). The biocompatibility of AM-CDs was assessed using the CCK-8 assay. Cells were initially plated into 96-well plates (1×10^5 cells/mL) in serum-free medium and allowed to adhere for 24 h. Subsequently, the cells were exposed to AM-CDs at a concentration gradient ranging from 7.81 to 1000 μg/mL for durations of 6, 12, 24, and 72 h. Post-incubation, the medium was discarded, and the wells were rinsed twice with PBS. Following the addition of 10 μL of the CCK-8 reagent, the plates were incubated for another 4 h, after which the absorbance was quantified at 450 nm. Cell viability was calculated as a percentage relative to the untreated control group. Cell viability is calculated using the following formula:

$$\text{Cell viability (\% of control)} = \frac{A_e - A_b}{A_c - A_b} \times 100 \quad (1)$$

A_e, A_b, and A_c represent the experimental, blank, and control groups.

4.12. Statistical Analysis

Data are expressed as mean ± standard deviation (SD). Statistical comparisons were performed using SPSS 26.0 software. One-way ANOVA or non-parametric tests were applied as appropriate, with intergroup differences analyzed by the LSD post hoc test. A

p value < 0.05 was considered statistically significant. The criteria for significance were defined as * $p < 0.05$, ** $p < 0.01$, and *** $p < 0.001$ vs. the corresponding control or model group, as indicated in each figure and table. For in vivo animal experiments, each group consisted of 8 biological replicates ($n = 8$). For in vitro cell experiments, each group was measured with three independent technical replicates.

5. Conclusions

In summary, we successfully engineered functional nitrogen and sulfur codoped carbon dots (AM-CDs) via a programmed pyrolysis of the *Acronicta major* larva. This strategy exemplifies a "Waste-to-Wealth" paradigm, effectively repurposing a destructive agricultural pest by eliminating its intrinsic biological toxicity while retaining its heteroatom-rich composition for in situ self-doping. The resulting AM-CDs exhibited excellent water solubility, distinctive fluorescence, and superior biocompatibility. Pharmacological evaluations demonstrated that AM-CDs possess potent sedative and hypnotic activities. In the PCPA-induced insomnia model, AM-CDs significantly alleviated sleep disturbances and anxiety-like behaviors, exhibiting efficacy but without inducing profound motor impairment. Mechanistically, this therapeutic effect is attributed to the restoration of neurochemical homeostasis, specifically characterized by the upregulation of inhibitory neurotransmitters (5-HT and GABA) and the suppression of excitatory glutamate levels. Collectively, this work provides a dual solution for ecological management and drug discovery. By validating the scientific basis of insect-derived nanotherapeutics, we offer a sustainable, green pathway for developing novel neuroprotective agents, transforming an ecological burden into a life-enhancing resource.

Supplementary Materials: The following supporting information can be downloaded at: https://www.mdpi.com/article/10.3390/molecules31040752/s1.

Author Contributions: Conceptualization, K.C. and J.M.; methodology, K.C.; software, X.T.; validation, K.C., X.T. and J.M.; formal analysis, K.C.; investigation, E.D.; resources, R.L.; data curation, M.X., B.J., S.W. and Z.L.; writing—original draft preparation, K.C.; writing—review and editing, Y.Z. (Yue Zhang); visualization, H.K.; supervision, H.Q.; project administration, Y.Z. (Yan Zhao); funding acquisition, Y.Z. (Yan Zhao). All authors have read and agreed to the published version of the manuscript.

Funding: This research is supported by the Fundamental Research Funds for the Central Universities (2024-JYB-JBZD-0400, 2024-JYB-JBZD-023, 2024-JYB-JBZD-045, 2025-XJ-KYQD-002).

Institutional Review Board Statement: The animal protocols were approved by the Committee of Ethics of Animal Experimentation of the Beijing University of Chinese Medicine (The ethics code is No. BUCM-2024122701-4261).

Informed Consent Statement: Not applicable.

Data Availability Statement: The original contributions presented in this study are included in the article/Supplementary Material. Further inquiries can be directed to the corresponding authors.

Conflicts of Interest: No conflict of interest was reported by the authors.

References

1. Early, R.; Bradley, B.A.; Dukes, J.S.; Lawler, J.J.; Olden, J.D.; Blumenthal, D.M.; Gonzalez, P.; Grosholz, E.D.; Ibañez, I.; Miller, L.P.; et al. Global threats from invasive alien species in the twenty-first century and national response capacities. *Nat. Commun.* **2016**, *7*, 12485. [CrossRef]
2. Wang, N.; Wang, W. Occurrence and control techniques of *Acronicta major*. *Shaanxi J. Agric. Sci.* **2016**, *62*, 127–128. (In Chinese) [CrossRef]

3. Cates, R.G. Feeding patterns of monophagous, oligophagous, and polyphagous insect herbivores: The effect of resource abundance and plant chemistry. *Oecologia* **1980**, *46*, 22–31. [CrossRef]
4. Chandrasekaran, M.; Mensah, R. Caterpillar dermatitis. *Indian Pediatr.* **2008**, *45*, 307.
5. Jadoo, A.S.; Treat, J.R. Caterpillar dermatitis: A brief report. *Pediatr. Dermatol.* **2020**, *37*, 570–571. [CrossRef]
6. Natsuaki, M. Immediate and delayed-type reactions in caterpillar dermatitis. *J. Dermatol.* **2002**, *29*, 471–476. [CrossRef] [PubMed]
7. Zhou, B.; Li, X. The monitoring of chemical pesticides pollution on ecological environment by GIS. *Environ. Technol. Innov.* **2021**, *23*, 101506. [CrossRef]
8. Kong, C.; Ren, L.; Shi, X.; Chang, Z. Soil pesticides pollution detection and specific recognition using electronic nose. *Sens. Actuator B-Chem.* **2024**, *408*, 135492. [CrossRef]
9. Ren, J.; Opoku, H.; Tang, S.; Edman, L.; Wang, J. Carbon dots: A review with focus on sustainability. *Adv. Sci.* **2024**, *11*, e2405472. [CrossRef] [PubMed]
10. Liu, J.; Li, R.; Yang, B. Carbon dots: A new type of carbon-based nanomaterial with wide applications. *ACS Cent. Sci.* **2020**, *6*, 2179–2195. [CrossRef] [PubMed]
11. Peng, C.; Chen, X.; Chen, M.; Lu, S.; Wang, Y.; Wu, S.; Liu, X.; Huang, W. Afterglow carbon dots: From fundamentals to applications. *Research* **2021**, *2021*, 6098925. [CrossRef]
12. Ge, G.; Li, L.; Wang, D.; Chen, M.; Zeng, Z.; Xiong, W.; Wu, X.; Guo, C. Carbon dots: Synthesis, properties and biomedical applications. *J. Mater. Chem. B* **2021**, *9*, 6553–6575. [CrossRef] [PubMed]
13. Xue, Y.; Wang, W.; Liu, Y.; Wang, J.; Walters, A.S. Sleep disturbances in generalized anxiety disorder: The central role of insomnia. *Sleep Med.* **2025**, *132*, 106545. [CrossRef] [PubMed]
14. Bourdet, C.; Goldenberg, F. Insomnia in anxiety: Sleep eeg changes. *J. Psychosom. Res.* **1994**, *38*, 93–104. [CrossRef] [PubMed]
15. Miller, N.S.; Gold, M.S. Benzodiazepines: A major problem. Introduction. *J. Subst. Abuse Treat.* **1991**, *8*, 3–7. [CrossRef]
16. Soyka, M. Treatment of benzodiazepine dependence. *N. Engl. J. Med.* **2017**, *376*, 1147–1157. [CrossRef]
17. Zhang, C.; Wang, X.; Shao, M.; Li, H.; Chen, Q.; Wang, N.; Xu, Q. Synthesis of nitrogen-enriched hydrochar via co-hydrothermal reaction of liquid digestate and corn stalk. *Sci. Total Environ.* **2022**, *836*, 155572. [CrossRef]
18. Yin, L.; Yang, Y.; Du, Z.; Duan, P.; Cao, C.; Kapusta, K. Recovery of organic materials from waste activated sludge for the rapid synthesis of n-doped hierarchical porous carbon as supercapacitor electrodes. *J. Environ. Manag.* **2025**, *384*, 125582. [CrossRef]
19. Kasif, M.; Alarifi, A.; Afzal, M.; Thirugnanasambandam, A. N, s-codoped carbon dots for antioxidants and their nanovehicle potential as molecular cargoes. *RSC Adv.* **2024**, *14*, 32041–32052. [CrossRef]
20. Rahman, M.M.; Byanju, B.; Lamsal, B.P. Protein, lipid, and chitin fractions from insects: Method of extraction, functional properties, and potential applications. *Crit. Rev. Food. Sci. Nutr.* **2024**, *64*, 6415–6431. [CrossRef]
21. Lopez-Santamarina, A.; Mondragon, A.D.C.; Lamas, A.; Miranda, J.M.; Franco, C.M.; Cepeda, A. Animal-origin prebiotics based on chitin: An alternative for the future? A critical review. *Foods* **2020**, *9*, 782. [CrossRef]
22. Ge, X.; Chen, R.; Deng, H.; Fang, L.; Pan, K.; Shan, B.; Gu, B.; Sun, X.; Zheng, Y.; Teo, B.K.; et al. Surface defects in atom-precise copper nanoclusters and their different catalytic efficiencies. *Nanoscale* **2025**, *17*, 25490–25494. [CrossRef]
23. Noble, F.; Roques, B.P. Assessment of endogenous enkephalins efficacy in the hot plate test in mice: Comparative study with morphine. *Neurosci. Lett.* **1995**, *185*, 75–78. [CrossRef]
24. Espejo, E.F.; Stinus, L.; Cador, M.; Mir, D. Effects of morphine and naloxone on behaviour in the hot plate test: An ethopharmacological study in the rat. *Psychopharmacologia* **1994**, *113*, 500–510. [CrossRef] [PubMed]
25. Gårdmark, M.; Höglund, A.U.; Hammarlund-Udenaes, M. Aspects on tail-flick, hot-plate and electrical stimulation tests for morphine antinociception. *Pharmacol. Toxicol.* **1998**, *83*, 252–258. [CrossRef] [PubMed]
26. Taghi Mansouri, M.; Naghizadeh, B.; Ghorbanzadeh, B.; Farbood, Y. Central and peripheral antinociceptive effects of ellagic acid in different animal models of pain. *Eur. J. Pharmacol.* **2013**, *707*, 46–53. [CrossRef]
27. de Sousa, D.P.; Nóbrega, F.F.F.; de Lima, M.R.V.; de Almeida, R.N. Pharmacological activity of (r)-(+)-pulegone, a chemical constituent of essential oils. *Z. Naturforschung C J. Biosci.* **2011**, *66*, 353–359. [CrossRef]
28. Guieu, R.; Harley, J.R.; Blin, O.; Pouget, J.; Serratrice, G. Nociceptive threshold in hypothyroid patients. *Acta Neurol.* **1993**, *15*, 183–188.
29. Amiri, M.; Esmaili, H.; Hamad, A.H.; Alavinia, M.; Masani, K.; Kumbhare, D. Nociceptive flexion reflex threshold in chronic pain patients: A needed update for the current evidence. *Am. J. Phys. Med. Rehabil.* **2021**, *100*, 750–759. [CrossRef] [PubMed]
30. Solomon, P.R.; Kiney, C.A.; Scott, D.R. Disruption of latent inhibition following systemic administration of parachlorophenylalanine (pcpa). *Physiol. Behav.* **1978**, *20*, 265–271. [CrossRef]
31. Park, D.H.; Stone, D.M.; Baker, H.; Kim, K.S.; Joh, T.H. Early induction of rat brain tryptophan hydroxylase (tph) mrna following parachlorophenylalanine (pcpa) treatment. *Brain Res. Mol. Brain Res.* **1994**, *22*, 20–28. [CrossRef] [PubMed]
32. Bubenik, G.A.; Pang, S.F. The effect of para-chlorophenylalanine (pcpa) on food consumption, food transit time and melatonin levels in the brain and the digestive tract of mice. *Comp. Biochem. Physiol. Comp. Physiol.* **1993**, *104*, 377–380. [CrossRef]

33. Keele, N.B. Phenytoin inhibits isolation-induced aggression specifically in rats with low serotonin. *Neuroreport* **2001**, *12*, 1107–1112. [CrossRef] [PubMed]
34. Hepsomali, P.; Groeger, J.A.; Nishihira, J.; Scholey, A. Effects of oral gamma-aminobutyric acid (gaba) administration on stress and sleep in humans: A systematic review. *Front. Neurosci.* **2020**, *14*, 923. [CrossRef]
35. Zhu, W.; Huang, L.; Cheng, H.; Li, N.; Zhang, B.; Dai, W.; Wu, X.; Zhang, D.; Feng, W.; Li, S.; et al. Gaba and its receptors' mechanisms in the treatment of insomnia. *Heliyon* **2024**, *10*, e40665. [CrossRef]
36. Wang, D.; Orser, B.A. Inhibition of learning and memory by general anesthetics. *Can. J. Anaesth. J. Can. D'anesthesie* **2011**, *58*, 167–177. [CrossRef]
37. Lu, L.X.; Yon, J.; Carter, L.B.; Jevtovic-Todorovic, V. General anesthesia activates bdnf-dependent neuroapoptosis in the developing rat brain. *Apoptosis Int. J. Program. Cell Death* **2006**, *11*, 1603–1615. [CrossRef]
38. Choi, C.H.; Chung, M.W.; Park, S.H.; Woo, S.I. Additional doping of phosphorus and/or sulfur into nitrogen-doped carbon for efficient oxygen reduction reaction in acidic media. *Phys. Chem. Chem. Phys. PCCP* **2013**, *15*, 1802–1805. [CrossRef]
39. Yan, F.; Jiang, Y.; Sun, X.; Bai, Z.; Zhang, Y.; Zhou, X. Surface modification and chemical functionalization of carbon dots: A review. *Mikrochim. Acta* **2018**, *185*, 424. [CrossRef] [PubMed]

Disclaimer/Publisher's Note: The statements, opinions and data contained in all publications are solely those of the individual author(s) and contributor(s) and not of MDPI and/or the editor(s). MDPI and/or the editor(s) disclaim responsibility for any injury to people or property resulting from any ideas, methods, instructions or products referred to in the content.